WATER RESOURCES RESEARCH, VOL. 36, NO. 10, PAGES 3063–3076, OCTOBER 2000

Boundary shear stress measurements in undular flows: Application to standing wave bed forms

H. Chanson

Department of Civil Engineering, University of Queensland, Brisbane, Queensland, Australia

Abstract. Waters flowing in natural streams and rivers have the ability to scour and to deposit materials, hence to change the bed topography. It is recognized that undular flows have great potential for sediment transport. In the present study, a fixed-bed model was used to investigate the spatial variations of boundary shear stress under standing waves (i.e., undular flow). The results (Figure 8) highlight the nonuniformity of the boundary shear stress distributions. Minimum boundary shear stress is observed under the wave crests, and maximum shear stress is observed under the wave troughs. The experimental findings suggest the formation of three-dimensional standing waves bed forms. Overall, the study highlights large variations of boundary shear stress in response to free-surface undulations.

1. Introduction

Waters flowing in natural streams and rivers have the ability to scour channel beds, to carry sediments, and to deposit materials, hence changing the bed topography. A proper understanding of river behavior is fundamental but yet not well understood, in particular the standing wave flow (Figures 1 and 2). It is recognized that undular flows have great potential for sediment dispersion: e.g., *Houk* [1934, p. 91] observed standing wave heights measured from crest to trough in excess of 4.5 m in a Denver waterway, and he noted, "the jump ... presented [a] repulsive appearance ... because of the presence of about 10 percent of black silt in the flow."

For Froude numbers close to unity a very small change in specific energy (e.g., caused by a bed irregularity) can induce a very large change of flow depth. The "unstable" nature of the flow is favorable to the development of large free-surface undulations or standing waves [e.g., *Imai and Nakagawa*, 1992; *Chanson and Montes*, 1995].

Undular flows in a movable boundary channel are associated with the formation of standing wave bed forms as it was observed when Figure 1 was taken. In the present study, a fixed-bed model was used to investigate the spatial variations of boundary shear stress. The results are then applied to gain a better understanding of the formation of standing wave bed forms associated with undular flows.

Few investigators studied undular bores [e.g., *Lemoine*, 1948; *Iwasa*, 1955], but most experimental studies of undular flows were performed with undular hydraulic jumps [e.g., *Darcy and Bazin*, 1865; *Chanson and Montes*, 1995], the present study being no exception. Pertinent studies included *Fawer* [1937] and, more recently, *Ryabenko* [1990], *Ohtsu et al*. [1995], and *Montes and Chanson* [1998]. These works showed that undular jumps may occur for upstream Froude numbers ranging from unity up to 3.5–4, corresponding to undular flow Froude numbers between unity and 0.35.

Undular hydraulic jumps are three-dimensional flows [e.g., *Darcy and Bazin*, 1865; *Fawer*, 1937; *Hager and Hutter*, 1984; *Chanson and Montes*, 1995]. The flow characteristics are functions of the upstream Froude number as well as the inflow conditions and aspect ratio d_c/W, d_c being the critical depth and W the channel width. *Henderson* [1966], *Rajaratnam* [1968], and *Leutheusser and Schiller* [1975] discussed the role of bottom roughness on the occurrence of free-surface undulations (Table 1). The experiments of Henderson and Leutheusser and Schiller suggested that undular flows above a rough bed take place for a wider range of Froude numbers compared to a smooth bed flow. Rajaratnam's observations were consistent with the trend.

In mobile-bed channels, *Tison* [1949] and *Simons et al*. [1961] investigated experimentally standing wave bed forms associated with free-surface undulations. *Kennedy* [1963] analyzed bed form migration (dunes and antidunes) including stationary bed forms (i.e., standing waves). He presented superb pictures of standing wave bed form formation. Recent publications attempted to relate the appearance of standing waves to a critical flow condition [e.g., *Grant*, 1997; *Tinkler*, 1997; *Chanson*, 1998]. This assumption is untrue, and experimental observations demonstrate that free-surface undulations may occur in numerous circumstances for which the flow is not critical (i.e., $Fr \neq 1$) but near critical (i.e., $0.3 \leq Fr \leq 3$), where Fr is the Froude number defined such as $Fr = 1$ at critical flow conditions [e.g., *Chanson*, 1996].

2. Experimental Apparatus

2.1. Presentation

The experiments were performed in a well-documented rectangular channel: over 90 different flow conditions were previously investigated [*Chanson*, 1993, 1995]. Details of the new experiments are listed in Table 1. The fixed-bed tilting flume (0.25 m wide, 20 m long) is made of glass bed and walls. During one series of experiments (series 2), a false perspex bottom and rough walls (embossed aluminium, stucco pattern, aluminium sheets manufactured by Alcan (product reference number KS05-10-1200-240-STU)) were installed. The embossed surface was 0.3 mm deep with a very smooth finish. (Surface inspection by electronic microscopy was performed at the University of Queensland to confirm this point.)

Paper number 2000WR900154.
0043-1397/00/2000WR900154$09.00

Figure 1. Standing wave flow on a beach, looking downstream with antidune flow in background.

Experimentally, the roughness height of the glass flume was estimated as $k_s = 0.01$ mm, and the equivalent roughness height of embossed aluminium walls was ~2 mm. (Such "hydraulic roughness" is produced by the embossed carved design.)

The water discharge was measured with a V notch weir. The percentage of error is expected to be <2%. The water depths were measured using a rail-mounted pointer gauge. Pressure, velocity, and bed shear stress distributions were recorded with a Prandtl-Pitot tube (design based upon Prandtl's tube: 3.35 mm external diameter, hemispherical nose). The translation of the gauge and Pitot tube in the direction normal to the channel bottom was controlled by a fine adjustment travelling mechanism (error <0.1 mm). The error on the transverse position of the gauge and tube is <0.5 mm, and the error on their longitudinal position is <2 mm.

For each experiment the start of the standing waves was located at least 10 m downstream of the channel intake. The supercritical inflow was fully developed and uniform equilibrium; that is, normal flow conditions were achieved. Pressure and velocity measurements were recorded at characteristic positions along the undular hydraulic jump: upstream of the jump (U/S), at the onset of the lateral shock waves (SW), at the first wave crest (1C), first wave trough (1B), and second wave crest (2C) (Figure 2a). Three series of experiments were performed: series 1 to study the flow field, series 2 to investigate the effect of rough sidewalls, and series 3 for boundary shear stress measurements (Table 1).

2.2. Calibration of the Prandtl-Pitot Tube

The boundary shear stress was measured with the Prandtl-Pitot tube used as a Preston tube. Prior to the experiments, the relationship between the boundary shear stress and Pitot tube reading was calibrated in situ in uniform equilibrium flows, and it was best fitted by

$$\tau_0 = 3.428 V_b^{1.654}, \quad (1)$$

where τ_0 is the boundary shear stress and V_b is the velocity measured by the Pitot tube lying on the boundary. Equation

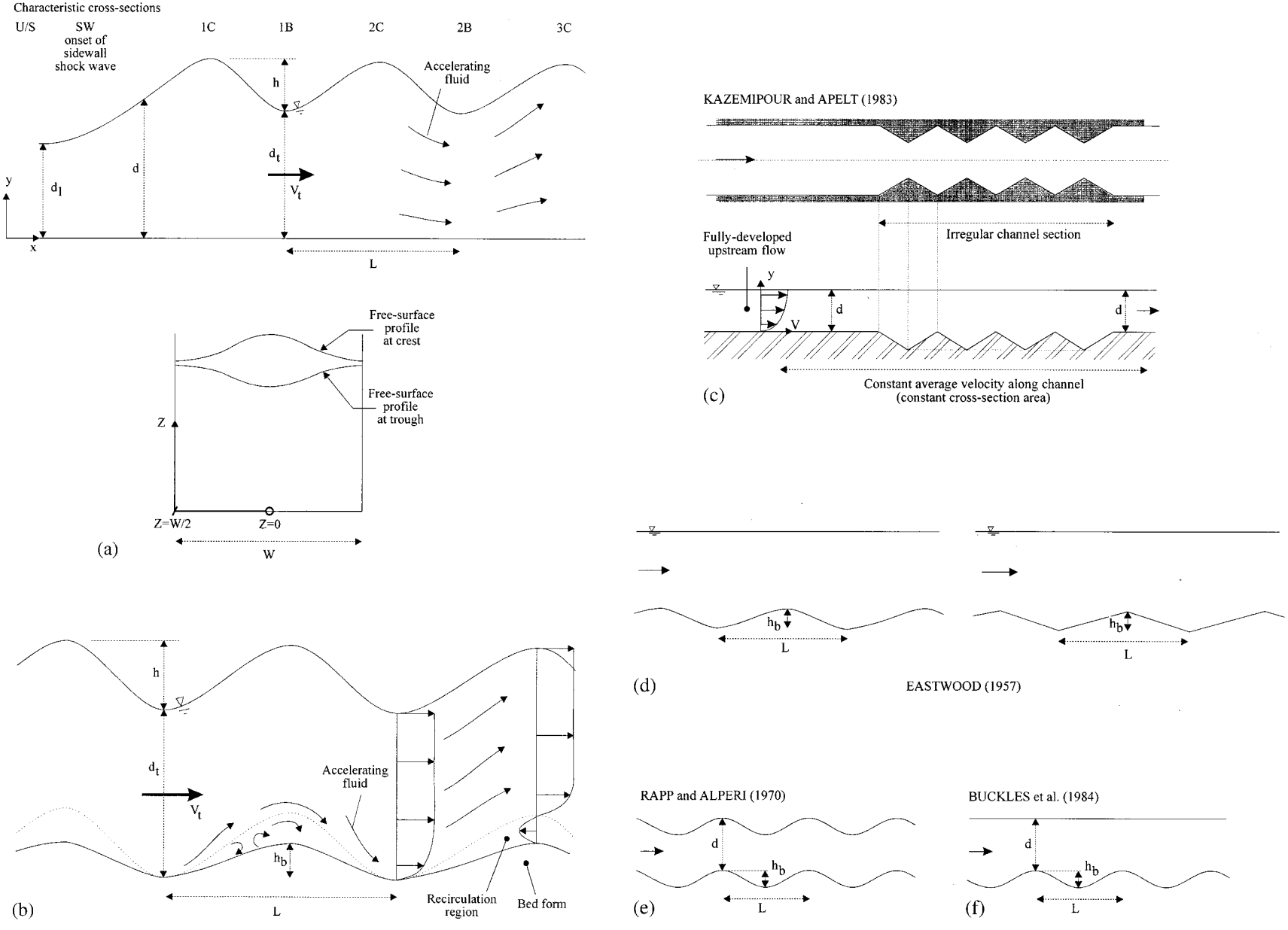

Figure 2. Sketch of undular flow above standing wave bed forms and related experimental channels (a) Present study, (b) undular flow above standing wave bed forms (c) *Kazemipour and Apelt* [1983], (d) *Eastwood* [1957], (e) *Rapp and Alperi* [1970], and (f) *Buckles et al.* [1984].

Table 1. Experimental Studies of Undular Flows (Fixed-Bed and Movable-Bed Channels)[a]

Reference/Run	θ, deg	d_1, m	Fr_1	d_c/W	Comments
			Fixed-Bed Channels		
Henderson [1966, pp. 216–217]	0	···	1.25–1.55	···	smooth and rough bottom
Rajaratnam [1968]					W = 0.311 m; glass sidewalls
Rajaratnam [1968]	···	0.036	4.46	0.313	roughness R1, wire mesh and k_s = 2.5 mm; roughness R2, wire mesh and k_s = 1.0 mm
Rajaratnam [1968]	···	0.017	6.3	0.184	roughness R3, wire mesh and k_s = 2.2 mm; roughness R4, wire mesh, and k_s = 2.25 mm; roughness R5, river gravel and k_s = 9.1 mm
Leutheusser and Schiller [1975]					W = 0.235 m; fully developed inflow conditions
Leutheusser and Schiller [1975]	0	···	1.4 and 1.7	···	aluminium bottom; glass sidewalls
Leutheusser and Schiller [1975]	0	0.06–0.08	1.7–3.0	~0.4–0.5	spherical roughness bottom elements (ϕ = 0.006 m) and k_s = 5.7 and 22.4 mm
Leutheusser and Schiller [1975]	0	0.05–0.09	1.5–2.5	~0.4–0.5	metal angle bottom elements (0.0076 m high, 0.0254 m high) and k_s = 80 mm
Present study					
Series 1					W = 0.25 m; glass bed and walls
Series 1	0.283	0.0656	1.14	0.286	
Series 1	0.328	0.0618	1.25	0.286	
Series 1	0.401	0.0587	1.35	0.286	
Series 1	0.435	0.0558	1.45	0.286	
Series 2	0.382	0.0840	1.31	0.403	W = 0.25 m; glass bed and walls.
Series 2	0.386	0.0860	1.27	0.406	W = 0.248 m; perspex bed; rough walls
Series 3					W = 0.25 m; glass bed and walls
Series 3	0.210	0.047	1.25	0.219	run BK_1
Series 3	0.304	0.042	1.48	0.219	run BK_2
Series 3	0.430	0.0771	1.48	0.403	run AF_1
Series 3	0.319	0.0861	1.252	0.403	run AF_2
			Movable-Bed Channels		
Tison [1949]	···	d = 0.035–0.05	Fr = 0.42–0.68	~0.03–0.05	d_{50} = 0.25 mm and W = 0.7 m.
Simons et al. [1961]	···	d = 0.059–0.30	···	···	d_{50} = 0.45 mm
Kennedy [1963]	···	d = 0.037–0.10	···	···	d_{50} = 0.23 and 0.55 mm

[a]Notes: d_c, critical flow depth; d_1, upstream flow depth; Fr_1, upstream Froude number; W, channel width; center dots denote information not available.

(1) is similar to the calibration curves obtained by *Preston* [1954] and *Patel* [1965] and *Macinstosh* [1990], who used the same experimental channel (Figure 3). Further calibration and verification tests were performed to check the instrument accuracy in uniform and nonuniform channels (see Appendix A for full details). The data accuracy is expected to be ~2% on dynamic and static pressures, 1% on local velocity, and 5% on boundary shear stress.

3. Experimental Results

3.1. Flow Field

3.1.1. Basic results. Undular flows are characterized by the development of free surface undulations over a long distance. Both field and laboratory experiments highlight the three-dimensionality of the flow (e.g., Figures 1 and 4, but also *Darcy and Bazin* [1865], *Fawer* [1937], *Chanson and Montes*

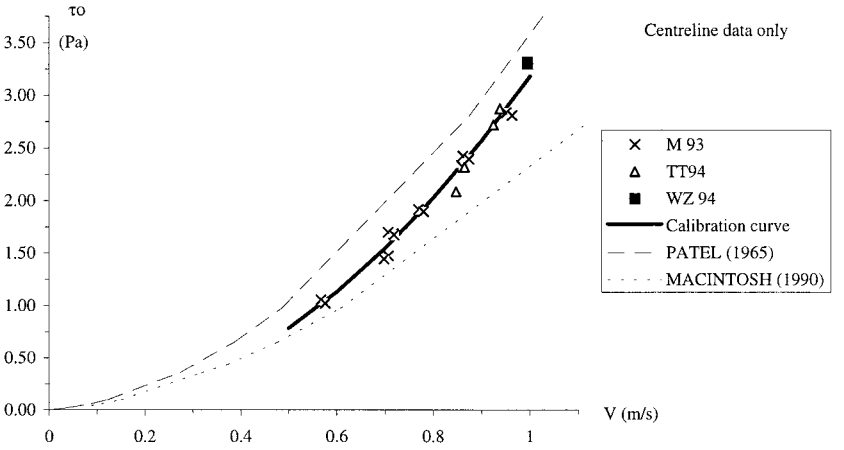

Figure 3. Calibration curve of the Prandtl-Pitot tube for boundary shear stress measurements.

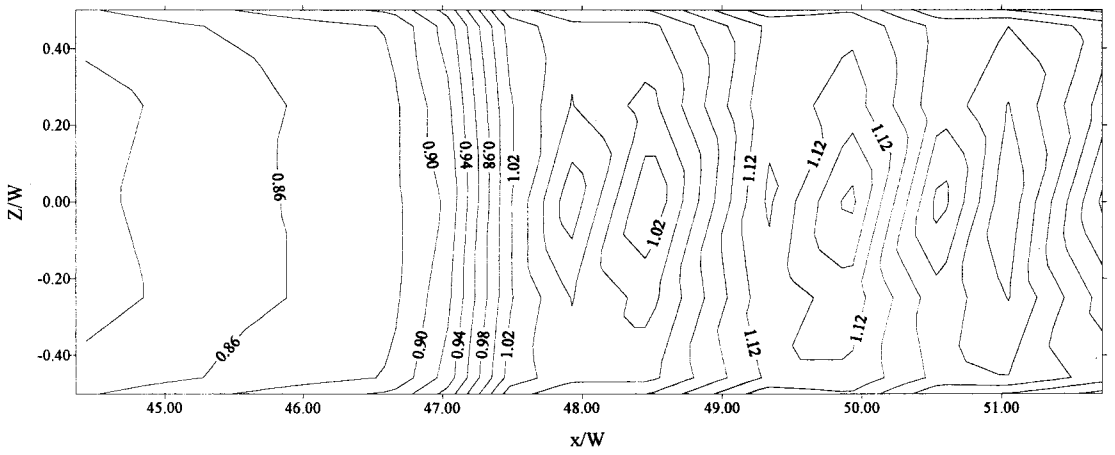

Figure 4. Dimensionless free-surface profile $\{x/W, Z/W, d/d_c\}$ for $q = 0.04$ m2/s and $d_c = 0.055$ m (run BK_1).

[1995], and *Ohtsu et al*. [1995], who used channel widths ranging from 0.25 to 2 m). In a straight prismatic channel the free-surface undulations are stationary and symmetrical around the channel centerline. Maximum wave amplitudes are recorded on the channel centerline, and the free-surface at the sidewalls follows the centerline flow pattern in phase with the same wave length but smaller amplitudes (e.g., Figure 4). The undular flow is consistently subcritical in average: that is, the ratio $Q/[g(A^3/W)]^2$ is less than unity, where Q is the flow rate and A is the flow cross section (Table 2). (In an undular hydraulic jump the undular region is defined as the flow region from and downstream of the first wave crest.) The pressure distribution is not hydrostatic in the undular region (e.g., Figure 5). The pressure gradient $\partial P/\partial y$ is less than hydrostatic at the wave crests and larger than hydrostatic at each wave trough. The largest deviations from the hydrostatic pressure distribution are observed on the channel centerline. Figure 5 presents an example of dimensionless pressure distributions with wave crest data in solid triangles and squares, trough data in open diamonds, the solid line being the hydrostatic pressure distribution. The variations in pressure distribution are consistent with the irrotational flow motion theory predicting larger than hydrostatic pressure gradient for concave (i.e., curved upward) free surfaces (e.g., trough) and less than hydrostatic for convex streamlines (e.g., crest) [e.g., *Rouse*, 1938; *Liggett*, 1994].

Dimensionless velocity distributions are presented in Figure 6. The data are plotted V/V_{max} versus y/d, where V is the local velocity at a distance y measured normal from the bed, d is the centerline depth, and V_{max} is the maximum velocity on the centerline. Figure 6 shows distributions on the centerline ($Z/W = 0$), in between the centerline and sidewall ($Z/W = 0.25$) and close to the sidewall ($Z/W = 0.46$), where W is the channel width and Z is the coordinate normal to the flow direction along the boundary ($Z = 0$ on centerline, $Z/W = 0.5$ at corner, and $Z/W > 0.5$ upward coordinate along the wall (Figure 2a)). All figures are plotted with the same scale, and the symbol legend is the same as for Figure 5. The data show basically that the fluid is decelerated upstream of each wave crest and accelerated downstream up to the wave trough. The effect is more pronounced close to the sidewall and next to the bed.

3.1.2. Discussion: Effect of wall roughness. For one set of flow conditions the effects of sidewall roughness were investigated. The free-surface pattern is modified with "steeper" lateral shock waves (that is, the flow depth discontinuity at the shock waves is greater with rough sidewalls) associated with some energy dissipation when they intersect at the first crest. It

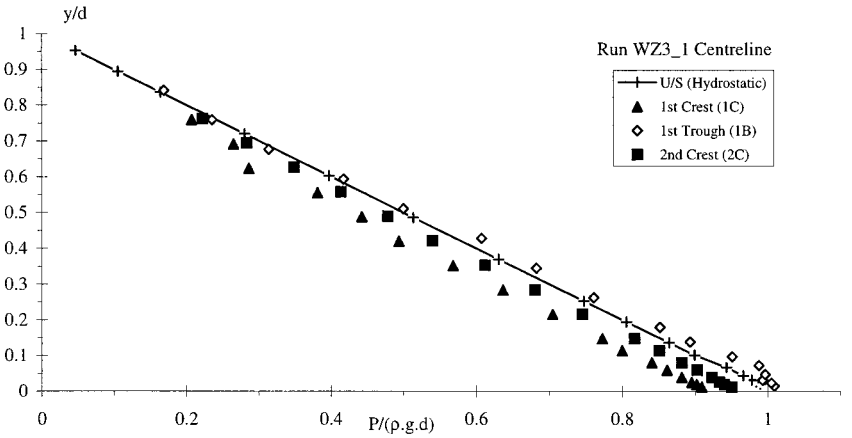

Figure 5. Dimensionless pressure distributions in undular flow for $q = 0.10$ m^2/s, $d_c = 0.101$ m, and $Fr_1 = 1.31$ (run WZ3_1).

Table 2. Experimental Results: Cross-Sectional Average Flow Properties (Experiments Series 3)[a]

	Run BK_1[b]				Run BK_2[c]				Run AF_1[d]				Run AF_2[e]			
Location	Dimensionless Longitudinal Distance[f]	Local Froude Number[g]	Dimensionless Average Boundary Shear Stress[h]	%SF Wall	Dimensionless Longitudinal Distance[f]	Local Froude Number[g]	Dimensionless Average Boundary Shear Stress[h]	%SF Wall	Dimensionless Longitudinal Distance[f]	Local Froude Number[g]	Dimensionless Average Boundary Shear Stress[h]	%SF Wall	Dimensionless Longitudinal Distance[f]	Local Froude Number[g]	Dimensionless Average Boundary Shear Stress[h]	%SF Wall
U/S	202.9	1.31	0.0034	0.19	155.2	1.51	0.0036	0.18	99.3	1.49	0.0037	0.37	99.3	1.26	0.0048	0.38
SW	223.8	1.22	0.0038	0.17	188.1	1.32	0.0036	0.18	103.3	1.30	0.0026	0.45	103.8	1.04	0.0050	0.41
1C	235.5	0.91	0.0039	0.21	196.1	0.77	0.0029	0.15	105.5	0.68	0.0020	0.27	105.9	0.67	0.0048	0.42
Half way 1C-1B	17.6	···	0.0039	0.21	21.2	···	0.0029	0.14	106.6	···	0.0026	0.35	107.4	···	0.0049	0.43
1B	240.6	0.96	0.0040	0.21	199.1	0.92	0.0037	0.17	107.8	0.71	0.0028	0.46	108.8	0.85	0.0050	0.42
Half way 1B-2C	20.8	···	0.0037	0.20	23.9	···	0.0026	0.16	109.3	···	0.0030	0.42	110.3	···	0.0046	0.42
2C	248.3	0.83	0.0038	0.20	206.8	0.69	0.0038	0.17	110.8	0.61	0.0031	0.47	111.9	0.64	0.0038	0.46
Half way 2C-2B	24.1	···	0.0043	0.21	27.4	···	0.0036	0.17								
2B	253.8	0.86	0.0043	0.20	213.0	0.84	0.0025	0.30								
Half way 2B-3C	26.9	···	0.0039	0.20	29.8	···	0.0026	0.19								
3C	259.6	0.78	0.0042	0.22	216.6	0.67	···	···								

[a]Notes: A, flow cross-sectional area; x, distance from channel intake; T_0, average cross-section boundary shear stress (equation (2)); %SF, percentage of total shear force carried by both sidewalls, U/S, upstream; SW, shock/wave; 1C, first crest; 1B, first trough; 2C, second crest; 2B, second trough; 3C, third crest.

[b]$Fr_1 = 1.25$; $q = 0.04$ m^2/s.

[c]$Fr_1 = 1.48$; $q = 0.04$ m^2/s.

[d]$Fr_1 = 1.48$; $q = 0.1$ m^2/s.

[e]$Fr_1 = 1.25$; $q = 0.1$ m^2/s.

[f]Dimensionless longitudinal distance is x/d_c.

[g]Local Froude number is $Q/[g(A^3/W)]^{1/2}$.

[h]Dimensionless average shear stress (dimensionless) is $T_0/0.5\rho(Q/A)^2$.

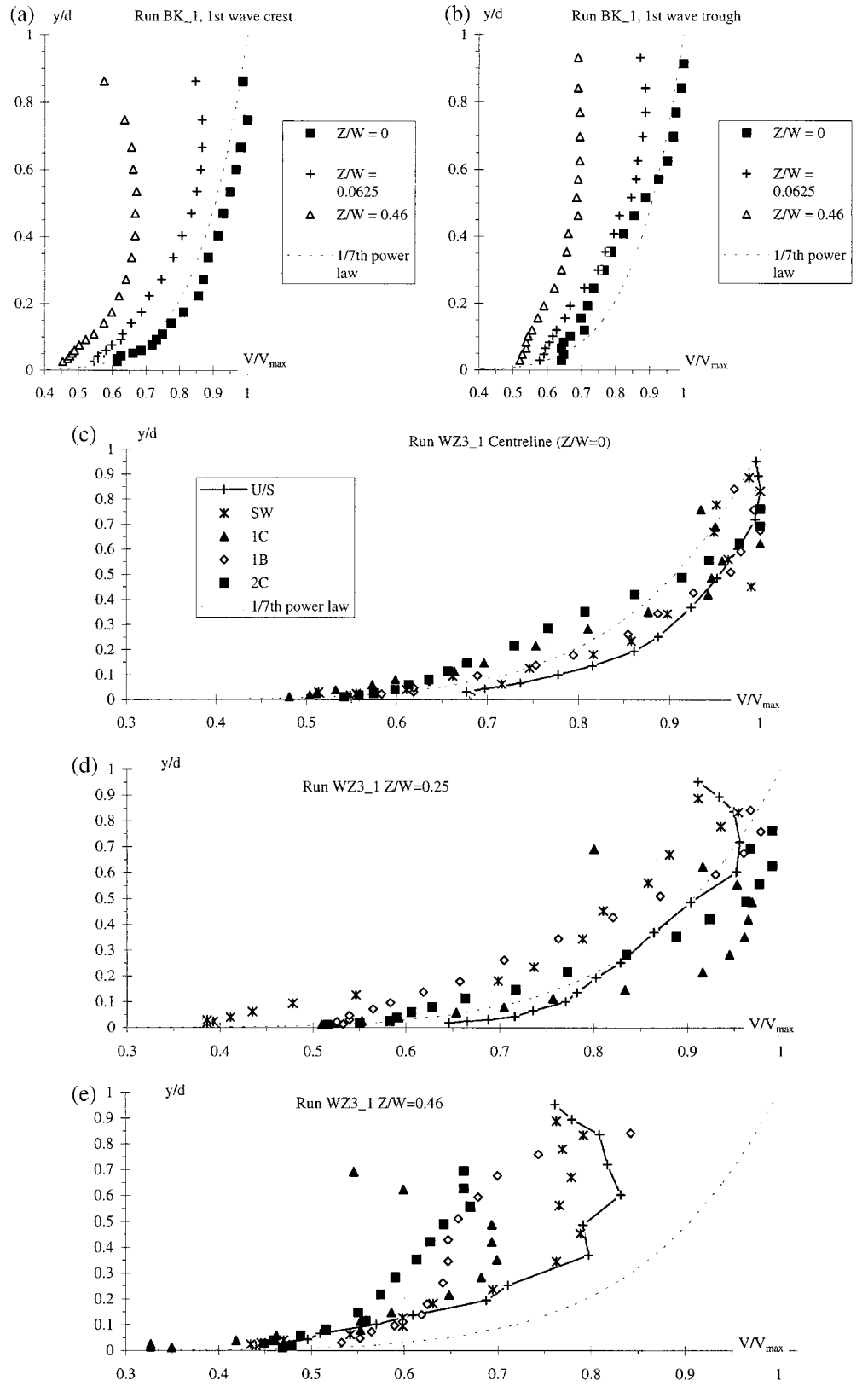

Figure 6. Dimensionless velocity distributions with $q = 0.04$ m^2/s, $d_c = 0.055$ m, and $Fr_1 = 1.25$ (run BK_1) for (a) first wave crest (centerline), with $V_{max} = 0.873$ m/s and d = 0.061 m, and (b) first wave trough (centerline), with $V_{max} = 0.869$ m/s and d = 0.0554 m. Dimensionless velocity distributions are also given with $q = 0.10$ m^2/s; $d_c = 0.101$ m; $Fr_1 = 1.31$ (run WZ3_1, smooth sidewalls); V_{max} (m/s) = 1.46 for upstream (U/S), 1.41 for shock wave onset (SW), 1.14 for first crest (IC) 1.17 for first trough (1B), and 1.03 for second crest (2C); and d(m) = 0.086 for U/S, 0.092 for SW, 0.147 for 1C, 0.121 for 1B, and 0.146 for 2C for (c) $Z/W = 0$ (centerline), (d) $Z/W = 0.25$, and (e) $Z/W = 0.46$. Another set of distributions is given with $q = 0.10$ m^2/s; $d_c = 0.101$ m; $Fr_1 = 1.27$ (run WZ3_2, rough sidewalls); V_{max} (m/s) = 1.45 for U/S, 1.39 for SW, 1.15 for 1C, 1.15 for 1B, and 1.04 for 2C; and d(m) = 0.086 for U/S, 0.091 for SW, 0.147 for 1C, 0.121 for 1B, and 0.147 for 2C for (f) $Z/W = 0$ (centerline), (g) $Z/W = 0.252$, and (h) $Z/W = 0.46$.

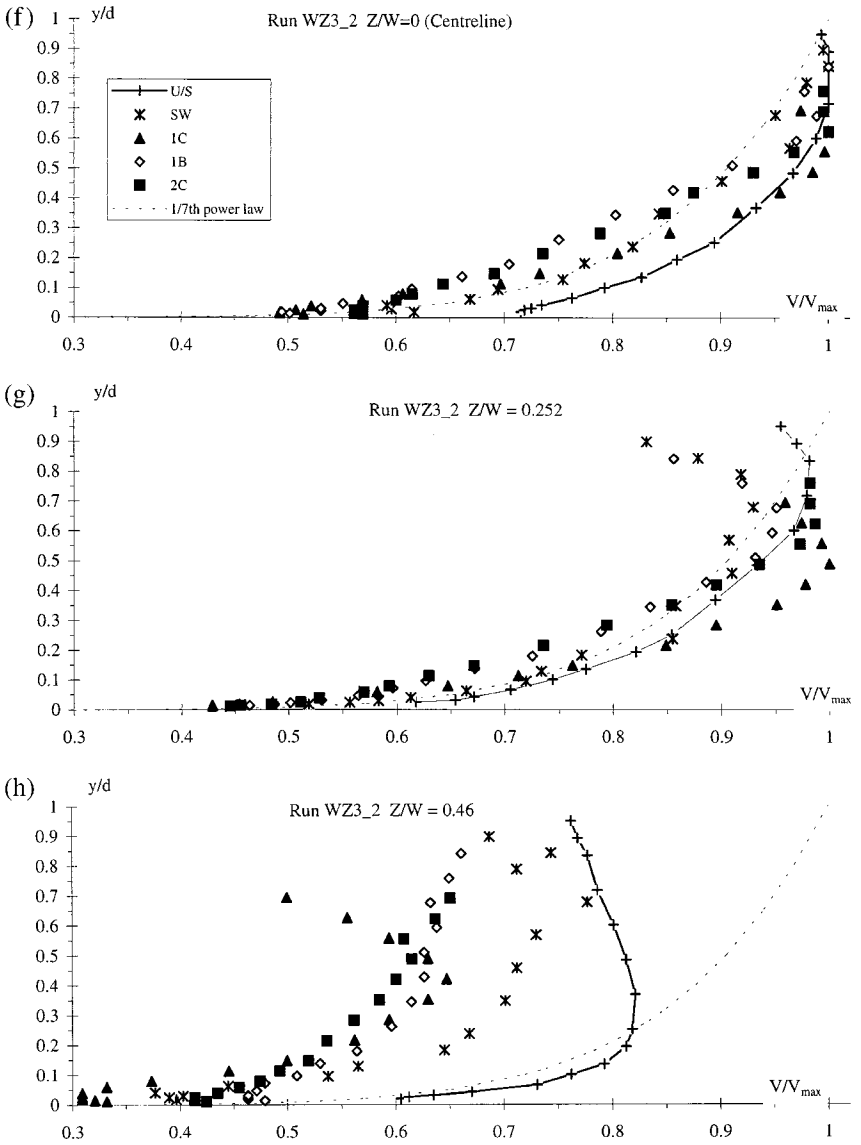

Figure 6. (continued)

is believed that the sidewall friction modifies the shockwave formation process [*Montes and Chanson*, 1998]. Changes in the velocity distributions are observed in the undular flow region, the largest differences being observed at the wave trough (Figure 6). It is possible that the present instrumentation was not accurate enough to detect small velocity variations in the slower wave crest flows. The sidewall roughness has, however, no substantial effect on the pressure distributions.

3.2. Boundary Shear Stress

The free-surface undulations are associated with significant variations of bed shear stress in the transverse and longitudinal directions. Experimental results are presented in Figures 7 and 8. Figure 7a shows transverse distributions of dimensionless boundary shear stress, while Figure 7b presents longitudinal profiles along the bed, in the corner, and along the sidewall, where x is the longitudinal distance from the channel intake. Figure 8 provides an overall picture of the bed and sidewall boundary shear stress distributions. Figure 8a presents a contour map for $Fr = 1.25$ (same flow conditions as Figure 4), and Figure 8b shows a surface for $Fr = 1.48$.

The results emphasize that the boundary shear stress distribution is not uniform in the undular flow region. Significant variations are observed both at the walls and on the bed. Minimum boundary shear stress is observed at wave crests, and maximum skin friction occurs at wave troughs. The findings are in agreement with the data of *Imai and Nakagawa* [1992]. For a given transverse position (i.e., Z = constant) the trough shear stress is about twice the wave crest shear stress.

3.2.1. Average boundary shear stress. At a given cross section (x = constant) the average wall shear stress T_0 may be defined as

$$T_0 = \frac{1}{P_w} \int_{-P_w/2}^{+P_w/2} \tau_0 \, dZ, \tag{2}$$

where P_w is the wetted perimeter. Experimental results for two inflow Froude numbers ($Fr_1 = 1.25$ and 1.48) and two flow

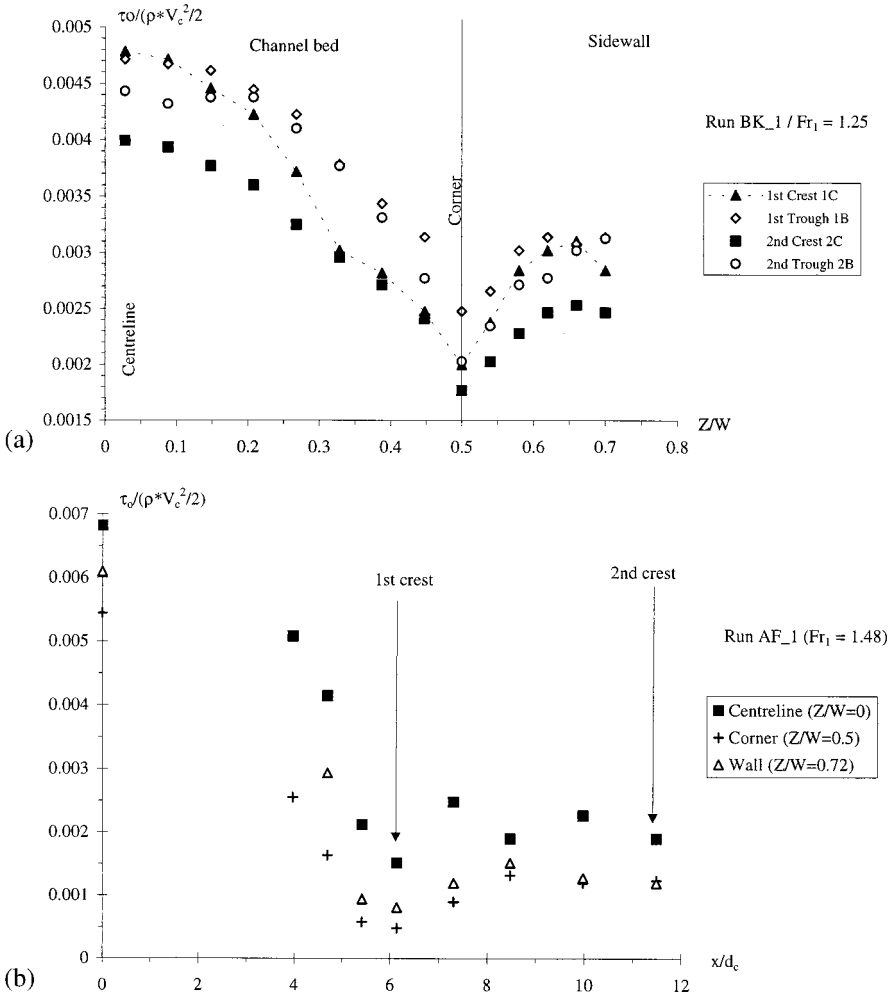

Figure 7. Dimensionless bed shear distributions $\tau_0/(0.5\rho V_c^2)$ for (a) transverse profiles, $q = 0.04$ m^2/s, $d_c = 0.055$ m, and $Fr_1 = 1.25$ (run BK_1), and (b) longitudinal profiles, $q = 0.1$ m^2/s, $d_c = 0.10$ m, and $Fr_1 = 1.48$ (run AF_1).

rates ($q = 0.04$ and 0.1 m^2/s) are summarized in Table 2. In Table 2 the shear force component carried by the sidewalls is shown. Although the data exhibit some scatter, it is conjectured that some error was caused by very slow fluctuations of the longitudinal position of the undular flow (fluctuation periodicity between 30 min and 3 hours approximately). Despite the scatter and for given flow conditions, the dimensionless mean boundary shear stress ($T_0/[0.5\rho(Q/A)^2]$) is about constant in the undular flow region: i.e., $T_0/[0.5\rho(Q/A)^2] = 0.0042$ and 0.0030 for $Fr_1 = 1.25$ and 1.48, respectively, independent of the flow rate and aspect ratio (Table 2).

Upstream of the hydraulic jump, the data of shear force applied to the walls are consistent results obtained in smooth rectangular channels for same aspect ratio W/d [*Knight et al.*, 1984]. In the undular flow, however, the sidewall shear force component is consistently lower than for smooth rectangular channels with identical aspect ratio W/d, where d is taken as the centerline flow depth (Table 2).

3.2.2. Longitudinal acceleration in undular flow. For a one-dimensional steady flow the momentum equation yields

$$\frac{1}{2}\frac{D_H}{\mathbf{V}}\frac{\partial \mathbf{V}}{\partial x} = -\frac{1}{2}\frac{gD_H}{\mathbf{V}^2}\frac{\partial z_0}{\partial x} - \frac{1}{2}\frac{D_H}{\rho\mathbf{V}^2}\frac{\partial P}{\partial x} - \frac{T}{\frac{1}{2}\rho\mathbf{V}^2}, \qquad (3)$$

where $\mathbf{V}$ is the mean flow velocity ($\mathbf{V} = Q/A$), z_0 is the channel bed elevation, D_H is the hydraulic perimeter, P is the average pressure in a cross section normal to the flow direction, and T is the total boundary shear stress. T includes the skin friction and form loss components:

$$T = T_0 + T_f, \qquad (4)$$

where T_f is the form-related shear stress and T_0 is the (measured) skin friction shear stress. In uniform equilibrium flows down a prismatic channel the terms $\partial\mathbf{V}/\partial x$ and $\partial P/\partial x$ are zero, and (3) yields the well-know result

$$\mathbf{V} = \sqrt{\frac{8g}{f}}\sqrt{\frac{D_H}{4}\left(-\frac{\partial z_0}{\partial x}\right)}, \qquad (5)$$

where f is the Darcy-Weisbach coefficient.

In undular flows the longitudinal flow acceleration term is consequent. Experimental data indicate that cross-section-averaged accelerations $(0.5D_H/\mathbf{V})(\partial\mathbf{V}/\partial x)$ range from -0.05 to $+0.06$ and depth-averaged centerline acceleration $(0.5d/V_m)$ $(\partial V_m/\partial x)$ are between -0.08 and $+0.06$, where V_m is the depth-averaged velocity. Larger accelerations were recorded next to the bed; that is, $(0.5d/V_b)$ $(\partial V_b/\partial x)$ =

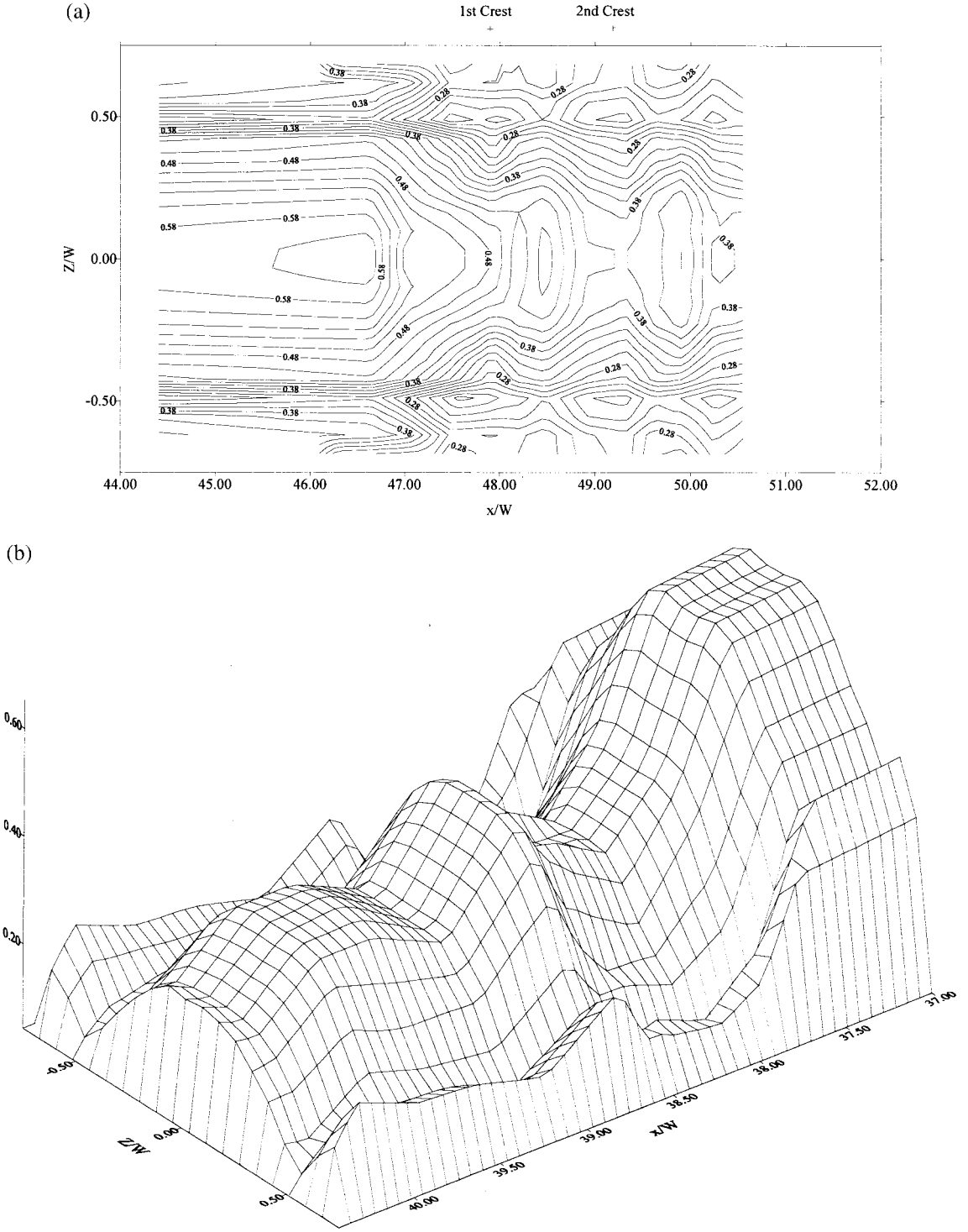

Figure 8. Bed shear stress contour map (x/W, Z/W, $\tau_0/(0.5\rho V_c^2)$ 100) for (a) $q = 0.04$ m^2/s, $d_c = 0.055$ m, and $Fr_1 = 1.25$ (run BK_1) with flow direction from left to right and (b) $q = 0.04$ m^2/s, $d_c = 0.055$ m, and $Fr_1 = 1.48$ (run BK_2) with flow direction from top right corner to bottom left.

-0.17 up to $+0.11$. The range of longitudinal acceleration data is independent of the inflow Froude number for experimental flow conditions such as $1.1 < Fr_1 < 2.4$. Altogether the maximum dimensionless accelerations are $\sim$1 order of magnitude larger than the average skin friction shear stress (Table 2).

3.3. Application to Standing Waves in Movable-Bed Channels

The experimental results show significant variations of the velocity and pressure distributions in undular open channel flows associated with large fluctuations of skin friction shear

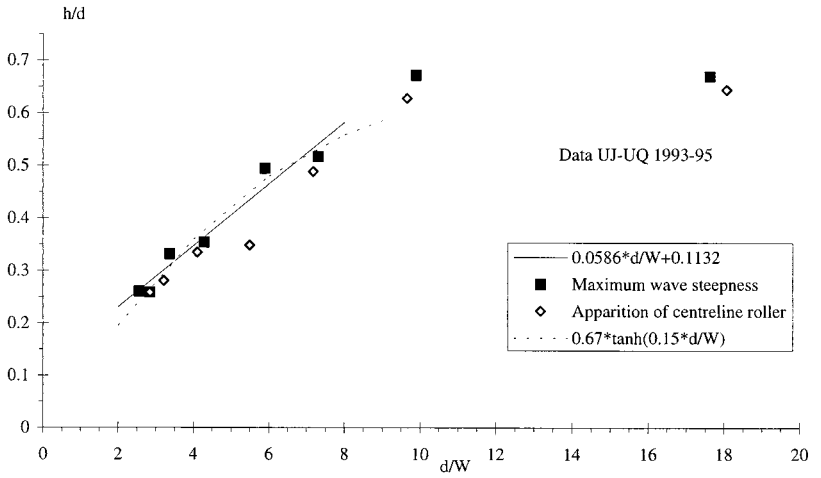

Figure 9. Maximum dimensionless wave height in undular flow.

stress in the longitudinal direction x and crosswise direction Z (Figures 5–7). They highlight the nonuniform variations of shear stress in response to the undular flow pattern. This suggests that the formation of standing wave bed form is the consequence of free-surface standing waves. Considering a flat movable-bed stream, an undular flow might take place during a flood event or near the estuary during a period of the tide. Below the free-surface standing waves the movable bed becomes subjected to a nonuniform boundary shear stress distribution (Figure 8). Erosion may take place underneath the wave troughs while accretion or lesser erosion may occur below the wave crests. This process leads to the formation of standing waves bed forms in phase with the free-surface standing waves.

The bed forms will not be two-dimensional. The boundary shear stress is consistently smaller at the sidewalls than on the channel centerline, and it is minimum in the corner ($Z/W = 0.5$) (Figure 8). Sediment motion will be more intense near the channel centerline than next to the banks. The boundary shear stress pattern implies the formation of three-dimensional bed forms. This result is consistent with *Kennedy*'s [1963] observations of standing wave bed forms. He noted the chaotic nature of the bed form life cycle [p. 522] "with a period of one to several minutes" and its [p. 542] "three-dimensional features."

The characteristic dimensions of standing wave bed forms are affected by the free-surface characteristics (see Appendix B). Maximum bed form height is associated with maximum free-surface wave height. In undular hydraulic jumps the dimensionless maximum wave height $(h/d)_{max}$ equals about 0.67 for wide channels, where d is the subcritical conjugate depth or average flow depth (Table 3 and Figure 9). For low aspect ratios the maximum wave height is related to the aspect ratio:

$$\left(\frac{h}{d}\right)_{max} \approx 0.67 \tanh\left(0.15\frac{d}{W}\right) \qquad 2 \leq W/d < 10. \quad (6)$$

In all cases, maximum wave height is associated with maximum wave steepness and the appearance of wave breaking, i.e., the apparition of a centerline roller called cockscomb roller by *Chanson and Montes* [1995]. The breaking wave height data are comparable with solitary wave breaking criterion. For a solitary wave, computational results suggested $(h/d)_{max} \approx 0.83$–0.85, but experimental results gave $(h/d)_{max} \sim 0.5$–0.75, which is close to the present results [e.g., *Massel*, 1996; *Dingemans*, 1997; *Montes*, 1998].

In movable-bed channels, *Kennedy* [1963] reported the occurrence of wave breaking for h/L between 0.13 and 0.16. His results are consistent with present observations of maximum wave steepness $(h/L)_{max}$ of ~0.12–0.13 in wide channel flows (Table 3).

3.4. Total Boundary Shear Stress in Undular Open Channel Flows

Movable-bed channels are characterized by a dual interaction between bed forms and flow resistance. *Kazemipour and Apelt* [1983] performed fundamental experiments in irregular open channels designed to operate with a constant mean flow velocity (Figure 2). Their results showed that the form losses could account for up to 92% of the total loss. Similar results were obtained both in open channels [*Eastwood*, 1957] and in wavy conduits [e.g., *Rapp and Alperi*, 1970; *Buckles et al*., 1984] with large pressure losses associated with form loss and recirculation motion (Figure 2). For two-dimensional bed form elements the bed form shear stress may be estimated as

$$T_f = \frac{1}{8}\rho V_t^2 \frac{(h - h_b)^2}{L\, d_t}, \quad (7)$$

where d_t and V_t are the flow depth and velocity at the wave trough, L is the wave length, h is the free-surface wave height, and h_b is the bed form height, assuming $h_b < h$ (Figure 2).

Table 3. Maximum Wave Height Flow Conditions in Undular Jump Flows[a]

Fr_1	$(h/L)_{max}$	$(h/d)_{max}$	Fr	d/W	Comments
1.58	0.120	0.670	0.66	17.62	$d_c/W = 0.075$
1.68	0.131	0.671	0.63	9.89	$d_c/W = 0.138$
1.45	0.093	0.517	0.71	7.30	$d_c/W = 0.172$
1.51	0.097	0.494	0.69	5.90	$d_c/W = 0.218$
1.39	0.077	0.354	0.74	4.28	$d_c/W = 0.286$
1.27	0.065	0.332	0.79	3.36	$d_c/W = 0.347$
1.23	0.049	0.259	0.82	2.84	$d_c/W = 0.403$
1.28	0.051	0.261	0.79	2.56	$d_c/W = 0.456$

[a]Notes: d, conjugate flow depth; Fr, conjugate Froude number. Data are from *Chanson* [1993, 1995] and present study.

Equation (7) is derived from the Borda-Carnot formula. A similar expression was previously developed by *Engelund* [1966] for dune bed forms [e.g., *Chanson*, 1999]. Equation (7) predicts form drag losses of the same order of magnitude as Rapp and Alperi's results for identical flow conditions but lower than the experimental data of Eastwood and Buckles et al. (The data of *Rapp and Alperi* [1970] yield $T/T_s = 3.8$ and 6.7 for $h_b/L = 0.07$ and 0.42, respectively, and Reynolds numbers ranging from 4.5×10^4 to 2.5×10^5, where T_s is the smooth turbulent flow shear stress (straight walls).)

In undular flows the sudden expansion downstream of the wave trough might be "crudely" analyzed using (7). Indeed, this flow region is sometimes (but not always) associated with recirculation next to the bed below the wave crest [*Montes*, 1986; *Yasuda et al*., 1993; *Montes and Chanson*, 1998]. Equation (7) overestimates the form drag when applied to undular jumps on flat bed (i.e., $h_b = 0$). This result implies that form drag might not be significant in undular flows.

4. Conclusion

The variations of boundary shear stress in undular flows were investigated in a fixed-bed channel. Measurements of pressure and velocity profiles show that the pressure distributions in the undular flow are not hydrostatic in undular flows and the velocity distributions are three-dimensional, with large longitudinal and transverse variations. The results (Figures 7 and 8) highlight further the nonuniformity of boundary shear stress distributions. Minimum boundary shear stress is observed under the wave crests, and maximum shear stress is observed under the wave troughs. The pattern is observed both along the bed and at the walls. The experimental findings suggest the formation of three-dimensional standing waves bed forms in response to the free-surface undulations. The bed form height in undular flow will reach a maximum associated with the apparition of wave breaking, and experimental observations of the onset of wave breaking are consistent with solitary wave results.

Longitudinal accelerations (and decelerations) are important between wave crests and troughs, and their dimensionless magnitude is larger than the dimensionless skin friction shear stress. Importantly, the form drag in undular flow may be significant, although the process is not well understood. The present study is only a first step toward a better understanding of standing wave bed forms in open channels. Further investigations should be conducted to understand the sediment transport in undular flow and to expand the pioneering work of *Kennedy* [1963].

Appendix A: Boundary Shear Stress Measurements With Pitot Tubes

The Pitot tube is named after Henri Pitot (1695–1771), French mathematician, astronomer, hydraulician, and a member of the French Académie des Sciences from 1724. He invented a tubular device to measure flow velocity in the Seine River (first presentation in 1732 at the Académie des Sciences). Ludwig Prandtl (1875–1953) was a German physicist and aerodynamicist who introduced the concept of boundary layer [*Prandtl*, 1904] and developed the turbulent "mixing length" theory. He developed an improved Pitot tube design which provides direct measurements of the total head, piezometric head, and velocity [e.g., *Howe*, 1949, pp. 194–196; *Troskolanski*, 1960, pp. 212–215]. The modified Pitot tube is sometimes called a Pitot-Prandtl or Prandtl design tube. The accuracy of the Pitot-Prandtl tube is ~1% of the differential pressure under correct conditions of pressure recording. Although the concept relies on the tube alignment with the streamline, the Prandtl design gives a differential pressure error <1% for angles of deviations within the limits ±17° [e.g., *Howe*, 1949, p. 195; *Troskolanski*, 1960, pp. 213–214]. Errors on the total pressure and static pressure are <2.5% within the limits ±10° [e.g., *Troskolanski*, 1960, p. 213]. The 3.3 mm diameter tube used by the writer is based on the Prandtl design, and it was compared with a British Standards design within 1% in a wind tunnel for $Re = 1 \times 10^5$ to 9×10^5. In open channel flows at uniform equilibrium (i.e., normal flow conditions) the integration of velocity distributions measured at various transverse positions satisfied the continuity equation within 5% for $q = 0.02$–0.10 m^2/s [e.g., *Chanson*, 1995]. Additional (but incomplete) tests performed in boundary layer water flows showed that the errors on the total pressure, static pressure, and velocity were <5% for pitch angles between −3.5 and +10°.

On the basis of a dimensional analysis, *Preston* [1954] showed that the skin friction is measurable with a Pitot tube lying on the boundary. He stressed that the tube diameter had to be <20% of the boundary layer thickness. His work was extended by *Patel* [1965], who suggested an accuracy of ±1.5%. For the past 40 years, methods were devised to refine boundary shear stress measurements using "Preston-type" tubes. The experience gained at the University of Queensland suggests that each tube must be calibrated independently, preferably in situ, rather than relying on Patel's correlations. In the particular case of Prandtl-Pitot tubes the distance between the total and static pressure tappings is a critical factor (13 mm in the present study). Large distances could lead to significant errors because the flow conditions would differ between the two locations.

Xie [1998] investigated open channel flows in uniform ($W = 0.4$ m) and nonuniform ($0.2 \leq W \leq 0.4$ m) channels with a geometry identical to that used by *Kazemipour and Apelt* [1983]. In nonuniform channel he showed that the shear stress error measured with a Pitot tube is <10% for yaw deviations within <10°. Using both a Pitot tube (Roving Preston Tube) and a two-component laser Doppler velocimeter system, he further demonstrated that the boundary shear stress in nonuniform channels is a function of the velocity gradient at the wall provided that separation does not occur [*Xie*, 1998, p. 215]: "The magnitude of the BSS [boundary shear stress] is proportional to the velocity gradient at the boundary."

Appendix B: Bibliographic Review of Standing Wave Dimensions

Kennedy's [1963] ideal fluid flow calculations implied that stationary standing wave bed forms occurs for $0.896 \leq Fr \leq 1.589$ with corresponding wave lengths in the range $7.13 \leq L/d \leq 15.9$ (Table B1). A comparison with several sets of experimental data showed that the dimensionless wave lengths equal

$$L/d \approx 2\pi Fr^2 \tag{B1}$$

(bed form analysis), where L is the wave length, d is the undular flow mean water depth, and Fr is the undular flow Froude number. However a reanalysis of *Tison*'s [1949] undular bed form data yields

Table B1. Characteristic Dimensions of Standing Waves (Bed Forms and Free Surface)[a]

Reference	Wave Characteristics	Comments
	Bed Forms	
Tison [1949]	$L/d \approx 1/43–22$; $h_b/d = 0.2$	laboratory data: $0.035 \leq d \leq 0.05$ m; $0.42 \leq Fr \leq 0.68$
Kennedy [1963]	$L/d = 2\pi Fr^2$; $h_b/L \approx 0.014$;	ideal fluid flow calculations of stationary standing waves: $0.896 \leq Fr \leq 1.589$; $7.132 \leq L/d \leq 15.87$; validated with laboratory data
	$h_b/h = \cosh(2\pi d/L) \cdot [1 - (2\pi/Fr^2\ L/d) \tanh(2\pi d/L)]$	
	Free Surface	
Ideal fluid flow	$L/d \approx 1.79/(1 - Fr)^{0.614}$; $h/d \approx 1.312\ (1 - Fr)$	linearization of Boussinesq equation [e.g., *Keulegan and Patterson*, 1940; *Andersen*, 1978] for $0.75 \leq Fr \leq 0.95$
Experimental data [*Chanson* 1993, 1995; present study]	$L/d \sim 11.1\ Fr^{3.5}$; $3.4 < L/d < 8.3$; $h/d \approx 1.312\ (1 - Fr)$	undular jumps; centerline free-surface data: $0.7 \leq Fr < 0.9$

[a]Notes: d, undular flow mean water depth; Fr, undular flow Froude number; h, free-surface wave height; h_b, bed form height; L, wave length.

$$L/d \approx 1.43–22 \qquad 0.42 \leq Fr \leq 0.68 \qquad \text{(B2)}$$

(bed form data). *Kennedy* [1963] suggested that the amplitude of free-surface wave and bed form wave are related by

$$\frac{h_b}{h} = \left[1 - \frac{2\pi}{Fr^2}\frac{L}{d}\tanh\left(\frac{2\pi d}{L}\right)\right]\cosh\left(\frac{2\pi d}{L}\right), \qquad \text{(B3)}$$

where h_b is the bed form height and h is the free surface wave height (measured form crest to trough).

Most researchers have agreed that the standing wave bed forms and free-surface undulations have the same wave length and are in phase. It is therefore relevant to investigate the free-surface wave dimensions. For wave amplitude small compared to the flow depth the linearization of the Boussinesq equation yields [e.g., *Andersen*, 1978; *Montes*, 1979]

$$L/d \approx 1.79/(1 - Fr)^{0.614} \qquad 0.7 \leq Fr < 0.9 \qquad \text{(B4)}$$

(free-surface data). A reanalysis of free-surface profile data [*Chanson*, 1993, 1995] gives

$$L/d \sim 11.1\ Fr^{3.5} \qquad 0.7 \leq Fr < 0.9 \qquad \text{(B5)}$$

(free-surface data), where Fr is the conjugate (subcritical) Froude number, although the correlation between data and (B4) and (B5) is poor [e.g., *Chanson and Montes*, 1995, Figure 9].

The wave height of free-surface undulations may be derived from Boussinesq theory [e.g., *Keulegan and Patterson*, 1940]. The results are well correlated with experimental observations in undular jumps for $Fr_1 < 1.3$:

$$h/d \approx 1.312(1 - Fr) \qquad 0.75 \leq Fr \leq 0.95 \qquad \text{(B6)}$$

(free-surface data), where d is the undular (conjugate) flow depth and Fr is the subcritical (conjugate) Froude number [e.g., *Chanson*, 1993; *Chanson and Montes*, 1995, Figure 10].

Notation

A, A' cross-section area (m^2).
d water flow depth measured normal to the channel bottom (m).
D_H hydraulic diameter (m), equal to $4A/P_w$.
d_c critical flow depth (m).
d_1 upstream flow depth (m).
Fr Froude number, defined as $Fr = 1$ at critical flow conditions (i.e., minimum specific energy).
Fr_1 upstream Froude number.
f Darcy-Weisbach friction factor.
g gravity acceleration (m/s^2).
h wave height measured from crest to trough (m).
h_b bed form wave height (m).
k head loss coefficient.
k_s equivalent roughness height (m).
L wave length (m).
P pressure (Pa).
Q water discharge (m^3/s).
q discharge per unit width (m^2/s).
V velocity (m/s).
V_b velocity measured next to the bed (m/s).
V_c critical flow velocity (m/s).
V_m depth averaged velocity (m/s), equal to $1/d \int_0^d V\,dy$
$\mathbf{V}$ mean flow velocity (m/s), equal to Q/A.
W channel width (m).
x longitudinal flow distance measured from channel intake (m).
y direction normal to the flow direction (m).
Z transverse distance from the channel centerline (m), equal to zero on centerline, $0.5W$ at corner, and $0.5W$ upward.
z_0 bed elevation positive upward.
θ channel slope.
ρ density (kg/m^3).
T total boundary shear stress (Pa).
T_f form drag boundary shear stress (Pa).
T_0 average boundary shear stress (Pa) defined as (2).
T_s boundary shear stress in smooth turbulent flow along a straight conduit (Pa).
τ_0 boundary shear stress (Pa).
ϕ diameter.

Subscript

b bed form characteristics.
c critical flow.
f form drag.
s smooth turbulent flow.
t wave trough flow conditions.

Acknowledgments. The writer acknowledges the helpful comments of his friend J. S. Montes (University of Tasmania). He thanks also C. J. Apelt (University of Queensland) and the anonymous reviewers for their helpful suggestions.

References

Andersen, V. M., Undular hydraulic jump, *J. Hydraul. Eng*., *104*(HY8), 1185–1188, 1978.

Buckles, J., T. J. Hanratty, and R. J. Adrian, Turbulent flow over large-amplitude wavy surfaces, *J. Fluid Mech*., *140*, 27–44, 1984.

Chanson, H., Characteristics of undular hydraulic jumps, *Res. Rep. CE146*, 109 pp., Dep. of Civ. Eng., Univ. of Queensland, Brisbane, Australia, Nov. 1993.

Chanson, H., Flow characteristics of undular hydraulic jumps: Comparison with near-critical flows, *Rep. CH45/95*, 202 pp., Dep. of Civ. Eng., Univ. of Queensland, Brisbane, Australia, June 1995.

Chanson, H., Free-surface flows with near-critial flow conditions, *Can. J. Civ. Eng*., *23*(6), 1272–1284, 1996.

Chanson, H., Discussion of "Critical flow in rockbed streams with estimated values for Manning's n," by K. J. Tinckler, *Geomorphology*, *25*, 279–282, 1998.

Chanson, H., *The Hydraulics of Open Channel Flows: An Introduction*, 512 pp., Edward Arnold, London, 1999.

Chanson, H., and J. S. Montes, Characteristics of undular hydraulic jumps: Experimental apparatus and flow patterns, *J. Hydraul. Eng*., *121*(2), 129–144, 1995.

Darcy, H. P. G., and H. Bazin, *Recherches Hydrauliques* Imprimerie Impériales, Paris, 1865.

Dingemans, M. W., *Water Wave Propagation over Uneven Bottoms*, *Adv. Ser. Ocean Eng*., vol. 13, World Sci., River Edge, N. J., 1997.

Eastwood, W., The effect of bed profile on the hydraulic losses in open channels, *Water Water Eng*., *61*(738), 334–337, 1957.

Engelund, F., Hydraulic resistance of alluvial streams, *J. Hydraul. Eng*., *92*(HY2), 315–326, 1966.

Fawer, C., Etude de quelques ecoulements permanents à filets courbes, thesis, 127 pp., Imprimerie La Concorde, Lausanne, Switzerland, 1937.

Grant, G. E., Critical flow constrains flow hydraulics in mobile-bed streams: A new hypothesis, *Water Res. Res*., *33*(2), 349–358, 1997.

Hager, W. H., and K. Hutter, On pseudo-uniform flow in open channel hydraulics, *Acta Mech*., *53*, 183–200, 1984.

Henderson, F. M., *Open Channel Flow*, MacMillan, Indianapolis, 1966.

Houk, I. E., Hydraulic jump phenomena at Denver, *Engineer*, Jan. 26, 91–93, 98, 1934.

Howe, J. W., Flow measurement, in *Proceedings of 4th Hydraulic Conference*, edited by H. Rouse, pp. 177–229, John Wyley, 1949.

Imai, S., and T. Nakagawa, On transverse variation of velocity and bed shear stress in hydraulic jumps in a rectangular open channel, *Acta Mech*., *93*, 191–203, 1992.

Iwasa, Y., Undular jump and its limiting conditions for existence, *Proc. Jpn. Natl. Congr. Appl. Mech*., *5*, 315–319, 1955.

Kazemipour, A. K., and C. J. Apelt, Effects of irregularity of form on energy losses in open channel flow, *Aust. Civ. Eng. Trans*., *CE25*, 294–299, 1983.

Kennedy, J. F., The mechanics of dunes and antidunes in erodible-bed channels, *J. Fluid Mech*., *16*(4), 521–544, 1963.

Keulegan, G. H., and G. W. Patterson, A criterion for instability of flow in steep channels, *Eos Trans. AGU*, *21*, 594–596, 1940.

Knight, D. W., J. D. Demetriou, and M. E. Hamed, Boundary shear in smooth rectangular channels, *J. Hydraul. Eng*., *110*(4), 405–422, 1984.

Lemoine, R., Sur les ondes positives de translation dans les canaux et sur le ressaut ondulé de faible amplitude, *Houille Blanche*, Mar.–Apr., 183–185, 1948.

Leutheusser, H. J., and E. J. Schiller, Hydraulic jump in a rough channel, *Water Power Dam Constr*., *27*(5), 186–191, 1975.

Liggett, J. A., *Fluid Mechanics*, McGraw-Hill, New York, 1994.

Macintosh, J. C., Hydraulic characteristics in channels of complex cross-section, Ph.D. thesis, 487 pp., Dep. of Civ. Eng., Univ. of Queensland, Brisbane, Australia, 1990.

Massel, S. R., *Ocean Surface Waves: Their Physics and Prediction*, *Adv. Ser. Ocean Eng*., vol. 11, World Sci., River Edge, N. J., 1996.

Montes, J. S., Discussion of "Undular hydraulic jump" by V. M. Andersen, *J. Hydraul. Eng*., *105*(HY9) 1208–1211, 1979.

Montes, J. S., A study of the undular jump profile, paper presented at 9th Australasian Fluid Mechanics Conference, Auckland, New Zealand, 1986.

Montes, J. S., *Hydraulics of Open Channel Flow*, 697 pp., Am. Soc. of Civ. Eng., New York, 1998.

Montes, J. S., and H. Chanson, Characteristics of undular hydraulic jumps: Results and calculations, *J. Hydraul. Eng*., *124*(2), 192–205, 1998.

Ohtsu, I. O., Y. Yasuda, and H. Gotou, Characteristics of undular jumps in rectangular channels, *Proceedings of 26th IAHR Congress*, vol. 1, edited by D. A. Ervine, pp. 450–455, Int. Assoc. for Hydraul. Res., London, 1995.

Patel, V. C., Calibration of the Preston tube and limitations on its use in pressure gradients, *J. Fluid Mech*., *23*, 185–208, 1965.

Prandtl, L., Über Flussigkeitsbewegung bei sehr kleiner Reibung, *Verh. Intl. Math. Kongr. 3rd*, Heidelberg, Germany, 1904. (*Natl. Advis. Comm. Aeronaut. Tech. Memo*., *452*, 1928.)

Preston, J. H., The determination of turbulent skin friction by means of pitot tubes, *J. R. Aeronaut. Soc. London*, *58*, 109–121, 1954.

Rajaratnam, N., Hydraulic jumps on rough beds, *Trans. Eng. Inst. Can*., *11*(A-2), I–VIII, 1968.

Rapp, R., and R. W. Alperi, Pressure loss in convoluted pipes, *Build. Syst. Des*., Apr. 26–28, 1970.

Rouse, H., *Fluid Mechanics for Hydraulic Engineers*, 422 pp., McGraw-Hill, New York, 1938.

Ryabenko, A. A., Conditions favorable to the existence of an undulating jump (in Russian), *Gidrotekhn. Stroit*., *12*, 29–34, 1990. (*Hydrotech. Constr. Engl. Transl*., 762–770, 1990.)

Simons, D. B., A. M. Richardson, and M. L. Albertson, Flume studies using medium sand (0.45 mm), *U.S. Geol. Surv. Water Supply Pap*., *1498-A*, 76 pp., 1961.

Tinkler, K. J., Critical flow in rockbed streams with estimated values for Manning's n, *Geomorphology*, *20*(1–2), 1997.

Tison, L. J., Origine des ondes de sable (ripple-marks) et des bancs de sable sous l'action des courants, paper presented at 3rd Meeting, Int. Assoc. for Hydraul. Res., Grenoble, France, Sept. 5–7, 1949.

Troskolanski, A. T., *Hydrometry: Theory and Practice of Hydraulic Measurements*, 684 pp., Pergamon, Tarrytown, N. Y., 1960.

Xie, Q., Turbulent flows in non-uniform open channels: Experimental measurements and numerical modelling, Ph.D. thesis, 339 pp., Dep. of Civ. Eng., Univ. of Queensland, Brisbane, Australia, 1998.

Yasuda, Y., I. O. Ohtsu, and H. Gotou, A few experiments on undular hydraulic jump (in Japanese), paper presented at 48th Annual Meeting, Jpn. Soc. of Civ. Eng., Japan, Sept. Tokyo, 1993.

H. Chanson, Department of Civil Engineering, University of Queensland, Brisbane, Queensland 4072, Australia. (h.chanson@mailbox.uq.edu.au)

(Received October 21, 1999; revised May 1, 2000;
accepted May 15, 2000.)